Reduction of ring artifacts caused by 2D anti-scatter grids in flat-panel CBCT

Santiago. F. Cobos [1,2], Hristo N Nikolov[1], Steven I Pollmann[1], and David W Holdsworth[1,2,3]
[1]Robarts Research Institute, Bone and Joint Institute;
[2]Department of Medical Biophysics, Schulich School of Medicine & Dentistry;
[3]Department of Surgery, Schulich School of Medicine & Dentistry.
University of Western Ontario, London, ON, N6A 5K8 CANADA

ABSTRACT

Two-dimensional anti-scatter grids (2D-ASGs) have been developed to selectively capture scattered photons while preserving image signal in flat-panel cone-beam CT systems (CBCT). However, 2D-ASGs affect the response of detector elements underneath grid-septa, producing grid-line artifacts (GLA), which render traditional gain-and-offset corrections ineffective. GLA in the projection images lead to ring-artifacts in CBCT reconstructions, which undermine the improvements in image quality associated with 2D-ASGs. We propose a novel implementation of an exposure-dependent gain-correction and notch-Fourier filtering of the projection data to minimize GLA-related ring-artifacts in CBCT. A pixel-by-pixel gain-factor was calculated by dividing the intensities of a flat-field image (with no-ASG) by the intensities of a flat-field image with added ASG, at different exposure levels. Exposure levels were modified using copper filtration of the x-ray beam at six-different thicknesses (0 to 2.5 mm, 0.5 mm increments). Exposure-dependent gain-factors were stored in a multidimensional array and pixel-by-pixel exposure response was characterized using non-linear curve-fitting. The exposure-dependent gain-correction was applied to 215 projection images of a 14 cm water phantom using a cobalt-chrome 2D-ASG. Residual faint grid-lines were removed using a customized Fourier-notch filter prior to Parker-weighted FDK reconstruction. Traditional gain-and-offset correction produced severe ring-artifacts (i.e., σ = 833.64 HU) when compared to the exposure-dependent gain correction (i.e., σ = 76.16 HU). Additionally, Fourier-notch filtering improved CT number accuracy by 43 HU. Our results suggest that characterization of the exposure-dependent response of GLA-affected pixels can minimize ring-artifacts and improve CT-number accuracy, thus eliminating some of the difficulties of 2D-ASG implementation in CBCT systems.

Keywords: Anti-scatter, grids, flat-panel, cone-beam CT, CBCT, ring-artifacts.

1. INTRODUCTION

Among the many solutions to reduce the detrimental effects of scatter in CBCT image quality (i.e., reduced soft-tissue contrast and CT number inaccuracies)[1,2], two-dimensional anti-scatter grids (2D-ASGs) have been recently investigated and proposed.[3-5] Manufacturing of 2D-ASGs has been enabled by recent developments in 3D-modelling and metal 3D-printing. The array of two-dimensionally focused through-holes, characteristic of this type of anti-scatter grid, provides improved scatter rejection performance while maintaining primary x-ray transmission. Unfortunately, the grid-septa and grid-intersections, placed on top of the x-ray detector, reduce the x-ray fluence of underlying pixels, causing grid-line artifacts (GLA).[6,7] Failure to correct GLA in the projection images leads to severe ring-artifacts in CBCT reconstructions.[6,7] Severe ring-artifacts undermine the improvements in image quality due to scatter-rejection and therefore compromise the feasibility of 2D-ASGs implementation in CBCT systems.

Metal 3D-printed 2D-ASGs can be designed with grid-septa as thin as 100 µm, which in theory, should allow for GLA to be removed using traditional gain-and-offset corrections.[3-5] The reason being, that clinically used x-ray detectors have isometric pixels in the range of 130-250 µm and therefore cannot be fully blocked by 2D-ASG septa nor intersections. In practice, several phenomena interfere with the required linear response of GLA-affected pixels for traditional gain-corrections to work. For instance, signal leaking from neighbor pixels, which might be less affected by GLA, varies depending on their signal intensity. Furthermore, not all pixels are affected to the same degree (due to the aliasing of 2D-ASG septa), which further decreases traditional gain correction effectiveness. Iterative total variation minimization methods have been described to reduce GLA in projection images, but these techniques do not address the

Medical Imaging 2020: Physics of Medical Imaging, edited by Guang-Hong Chen, Hilde Bosmans, Proc. of SPIE
Vol. 11312, 1131228 · © 2020 SPIE · CCC code: 1605-7422/20/$21 · doi: 10.1117/12.2548778

phenomenological cause of GLA persistence. We believe that characterization of the exposure-dependent response of GLA-pixels and the development of an adaptive-gain scheme can ameliorate the negative effects of GLA in CBCT reconstructions. In this paper, we hypothesize that GLA affect the response of flat-panel detector pixels, which renders traditional gain-and-offset corrections ineffective. We describe a novel implementation of an exposure-dependent gain-correction and notch-Fourier filtering of the projection data to minimize GLA-related ring-artifacts in CBCT.

2. METHODOLOGY

2.1 Experimental setup

A 245x294x10 mm 2D-ASG was manufactured from cobalt-chrome alloy using high-resolution powder-bed fusion (AM400, Renishaw plc). The ASG had a square profile with a pitch of 9.09 lines/cm and 10:1 grid ratio. The nominal 0.1 mm grid septa were focused to a 732 mm x-ray source. The 2D-ASG was coupled to a 0.139 mm element pitch flat-panel detector (DRX-Plus 3543, Carestream Health) and proper alignment was confirmed by consistent grid line shadow thickness across the whole detector array. A 140 mm CBCT image quality phantom was imaged using a rotary stage and a ceiling mounted x-ray unit (Proteus XR/a, GE Medical Systems, 80kVp, 0.5mAs).

2.2 Exposure-dependent gain characterization

Traditional gain-and-offset correction, which is regularly used to reduce pixel-to-pixel response variations in digital x-ray detectors, was not able to correct GLA intensity in projection images using a 2D-ASG. The traditional approach fails because the gain-factor of pixels covered by grid-lines, varied depending on exposure levels. Gain-factors, G(x,y), for traditional corrections for an exposure level I were calculated as follows:

$$G(x,y,I) = \frac{P(x,y)}{I(x,y)} \tag{1}$$

Where P(x,y) is the intensity value measured in arbitrary digital units (ADUs) of a flat-field image with no-ASG, and I(x,y) is the intensity value of a flat-field image in ADUs with ASG. Figure 1 shows the exposure-dependent variation in gain-factors for three groups of pixels: unaffected by grid-artifacts, affected by grid-septa, and affected by grid-intersections at different exposure levels. Exposure levels were modified using copper filtration of the x-ray beam at six different thicknesses (0 to 2.5 mm, with 0.5 mm increments).

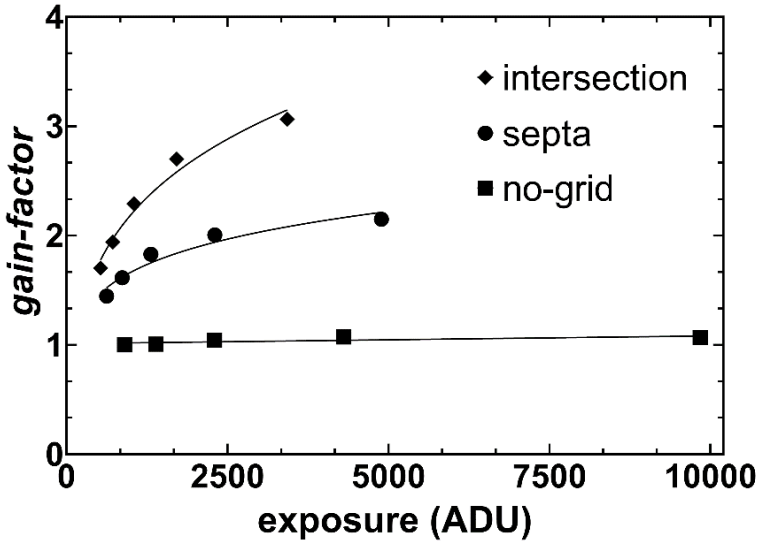

Figure 1. Exposure-dependent gain-factor variations for different cases of detector elements affected by grid-line artifacts. Power series curve-fits are shown in solid lines.

2.3 Adaptive-gain correction

Gain-factors were calculated for each pixel (x, y) at different exposure levels and the data was stored in a multidimensional array (3072x2560x6) using Matlab (MATLAB, The MathWorks, Natick). Pixels unaffected by grid-artifacts had gain-factors that remained constant (i.e., standard deviations < 0.05) between exposures, whereas pixels affected by grid-artifacts described a power function, $f(x) = a\,(ADU)^b + c$ (Fig. 1). For such cases, curve coefficients were calculated using MATLAB and stored in a look-up table that was used to assign a gain-factor profile for each pixel before CBCT data image acquisition. Projection images were then corrected using pixel specific adaptive-gain correction. Altunbas et al.[7] implemented a similar approach to identify and correct small clusters or structured line patterns in flat-panel detectors caused by pixels exhibiting non-linear responses to x-ray exposure (i.e. inherent to the detector). To the best of our knowledge, our current work is the first time such an adaptive-gain correction has been implemented for the case of pixels which respond non-linearly due to GLA. Figure 2 shows the results of traditional gain correction versus the adaptive-gain scheme.

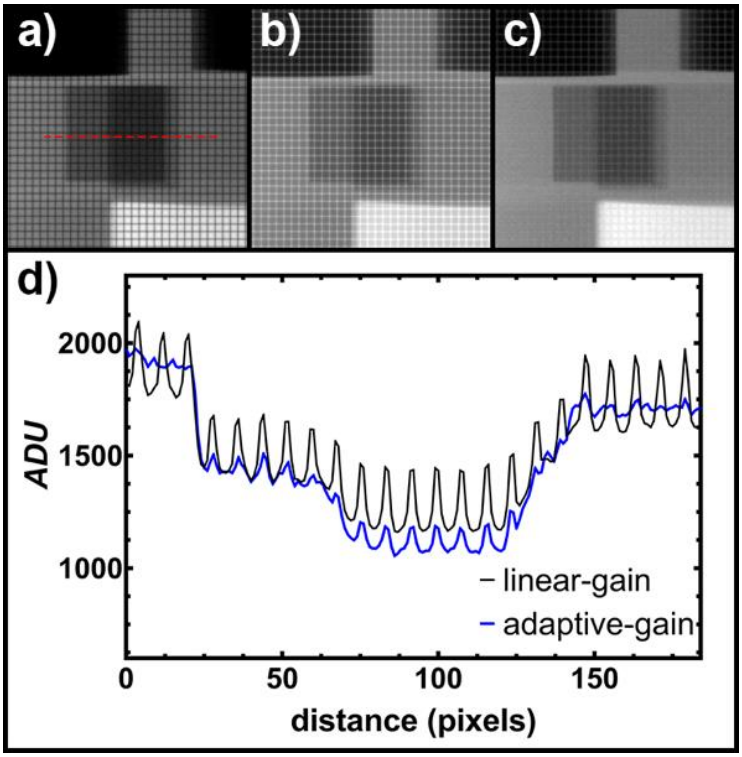

Figure 2. Close-up of QA phantom region in a CBCT 2D projection image: a) raw grid-line artifacts, b) after linear-gain correction, and c) using adaptive-gain correction. d) line-profiles (red-dotted line) showing the reduction of GLA intensity using the proposed method.

2.4 Additional frequency filtration

faint grid-line artifacts remained visible in the projection images even with careful characterization of the response of grid-affected pixels. However, the regular spatial frequency of the grid-line artifacts allowed implementation of a customized fast-Fourier-transform (FFT) notch filter that resulted in further reduction of GLA.[8] Only gridlines were affected by the FFT filter, because no other structures presented the same spatial frequency in the projection data.

2.5 Cone-beam CT image reconstruction

Two-hundred and fifteen (215) projection images of the CBCT quality control phantom,[9] with a 2D-ASG in place, were used to reconstruct a CBCT volume using a Parker-weighted FDK algorithm. The full-resolution volumes were calibrated to Hounsfield units (HU), and spatially averaged to a clinically acceptable voxel size (357x357x357 μm) to improve signal-to-noise characteristics of the data.[11]

2.6 Performance assessment

As previously mentioned GLA in projection images lead to severe ring artifacts in CBCT reconstructions. Therefore, reconstructed regions affected by ring-artifacts present large mean pixel standard deviations (SD). SD values were calculated using regions of homogeneous material near the center of rotation of the resolution plate of the QA phantom image reconstruction. This plate (consisting of aluminum-plastic bar patterns) was also used to qualitatively assess image sharpness. Additionally, the contrast plate of the QA phantom was used to further quantify improvements in image quality by calculating the contrast-to-noise ratio (CNR) for multiple inserts. CNR was calculated using the following:

$$CNR = \frac{|C - B|}{\frac{1}{2}\sqrt{\sigma_C^2 + \sigma_B^2}} \tag{2}$$

were C is the average pixel value of the insert, B is the average pixel value of the background, σ_C is the standard deviation of insert pixels, and σ_B the standard deviation of background pixels. Finally, improvements in CT number accuracy were analyzed by visualizing pixel variations across an air-filled chamber inside the QA phantom.

3. RESULTS

3.1 Ring-artifact reduction

Traditional linear-gain correction produced severe ring-artifacts (i.e., σ = 894.02 HU) when compared to the exposure-dependent gain-correction (i.e., σ = 85.55 HU) for homogeneous regions of the QA phantom. Additionally, Fourier-notch filtering improved CT number precision by 31 HU. Qualitative analysis of line-pairs showed that ring removal had little effect on image spatial-resolution (Figure 3).

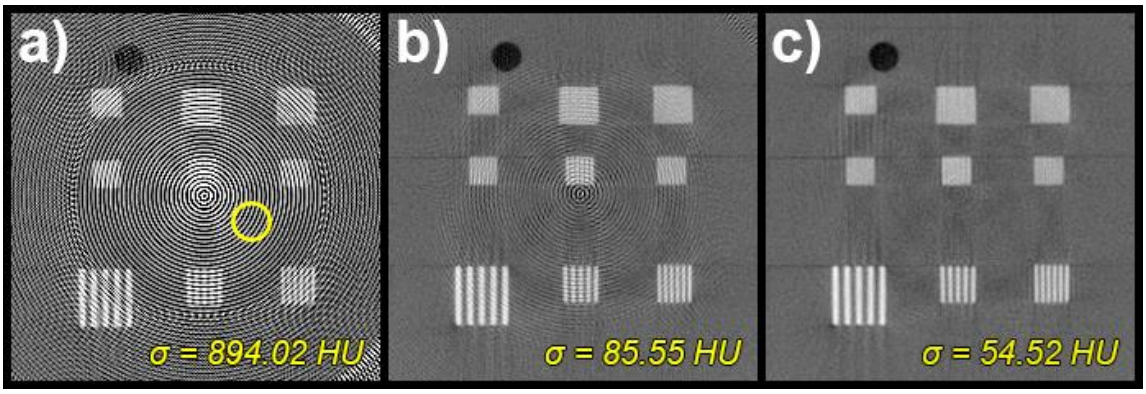

Figure 3. Resolution plate of QA phantom reconstructed a) using linear-gain correction, b) using adaptive-gain, and c) after Fourier-notch filtering. Standard deviations of the outlined ROI show improvements in image quality using the proposed method.

3.2 Improvements in contrast-to-noise ratio (CNR)

Contrast-to-noise ratio (CNR) for inserts with different iodine concentrations inside the QA phantom were significantly improved by the adaptive-gain method and faint-ring artifacts were removed by Fourier-notch filtering. Figure 4 (b-c), shows improvements in object visualization, which is attained by a decrease in image noise caused by the 2D-ASG. In contrast, Figure 4 (a), shows severe ring artifacts undermining the improvements in image quality associated with 2D-ASGs.

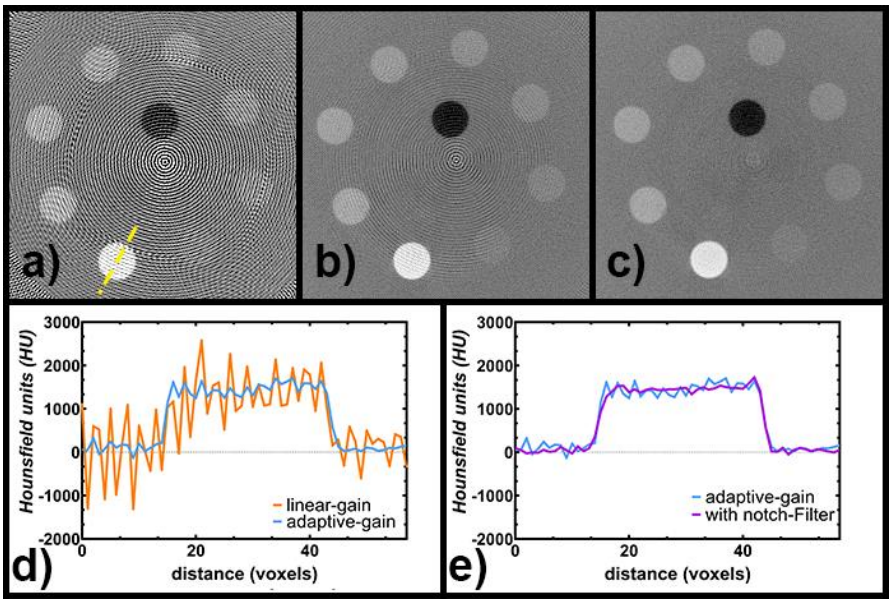

Figure 4. Improvements in CNR for inserts with different iodine concentrations a) image reconstruction using linear-gain correction b) using adaptive-gain correction, and c) after Fourier-notch filtering. d-e) line-profiles (yellow-dotted line) across iodine insert for quantitative assessment of CNR.

3.3 Improvements in CT number accuracy

Improvements in CT number accuracy for homogeneous materials were observed by analyzing HU variations across an air-filled slanted-edge chamber inside the QA phantom. Ring-artifacts caused by GLA were significantly minimized and faint-rings removed by Fourier filtering. Figure 5 (b-c), show low-HU variations, ~50 HU, after implementation of the proposed methods.

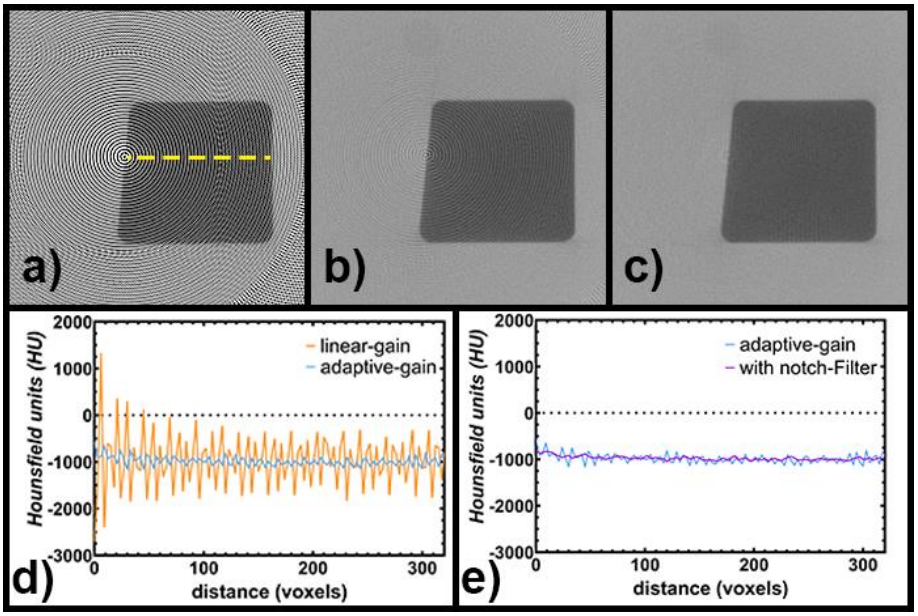

Figure 5. CT number accuracy improvements for air-filled slanted edge chamber inside the QA phantom. a) reconstruction with traditional gain correction b) with adaptive-gain, and c) using Fourier filtering. d-e) show line profiles across the air-filled structure.

4. CONCLUSIONS

4.1 Exposure-dependent response

As hypothesized, our results show that GLA-affected pixels do not respond linearly to different exposure levels. Figure 1 shows how pixels covered by grid-intersections or grid-septa require different gain-factors (depending on exposure levels), while gain-factors for un-affected pixels remind constant. Traditional gain-corrections overestimate gain-factors in regions of low-signal intensity. For instance, in Figure 2 (b) the central region of the image shows a relatively dense object where pixels affected by GLA appear to have a higher intensity value than the non-GLA affected pixels. Figure 2 (c) shows the improvements in GLA using an adaptive-gain. We believe that our proposed method can be implemented in combination with any GLA reduction scheme that requires a gain-and-offset step. Furthermore, our correction scheme might benefit other ASG applications that usually require reciprocating hardware to remove GLA.

4.2 Adaptive-gain scheme

The proposed adaptive-gain scheme was able to significantly reduce the intensity of GLA in projection images and therefore reduced the intensity of ring-artifacts in CBCT reconstructions. Characterization of the exposure-dependent response for pixels affected by GLA can be easily implemented in any CBCT system that allows geometrically stable coupling between the detector and the 2D-ASG. Other methods to reduce GLA, including total-variation based suppression, rely on the use of binary maps that label pixels only as affected or non-affected by GLA. As discussed before, this approach neglects the various degrees by which pixels might be affected by GLA (i.e., grid-septa aliasing). The adaptive-gain scheme implements a correction curve for each individual pixel affected by GLA, which makes it more flexible and robust. Another advantage of the proposed method is that it does not require any iterative or computationally intensive steps. Once the calibration has been done, the associated look-up table can be used to efficiently correct GLA in all the projection images, provided that the geometry of the CBCT system is not altered.

4.3 Limitations

The implementation described here was on a custom-built CBCT system with a stationary detector and grid. In a gantry-mounted system, mechanical imperfections (i.e., gantry sag) may modify the relationship between the x-ray source, the 2D-ASGs, and the flat-panel detector. Consequently, GLA might present small but significant shifts at different angles of the gantry, which may compromise GLA corrections. Other studies have shown that mechanical instabilities are reproducible and angle-dependent.[10] Therefore, we believe this problem can be ameliorated by calibrating the detector response, using angle-dependent look-up tables.

Periodic GLA can be filtered in the frequency domain, as long as the GLA appear at relatively high spatial frequencies. On the contrary, if the GLA pitch has a lower spatial frequency (i.e. > 2 mm pitch) Fourier filtration might impact the image information of the object. We have not implemented the described adaptive-gain scheme in any large pitch 2D-ASGs (i.e. < 5 lines cm^{-1}) but we believe Fourier filtration might not be required, as GLA will affect a significantly lower number of detector elements. Another important aspect to consider when designing 2D-ASGs has to do with the ratio of septal width to detector pixel size. For instance, as the septal width increases, GLA affect a larger area of the detector, becoming more intense and difficult to correct. GLA intensity will also increase if pixel size is close to septal width. In our study, no pixel received less than 30% of primary signal and therefore we cannot extrapolate the effectiveness of our adaptive-gain scheme to situations where the ratio of septal width to pixel size is less optimal. It is worth noting that one of the main reasons for using a customized CBCT setup was to test the feasibility of the 2D-ASG coupled with a clinically relevant flat-panel detector (DRX-Plus 3543, Carestream Health), allowing us to test our approach with a pixel size appropriate for diagnostic imaging (i.e. 139x139 µm).

Finally, although recently reported 2D-ASGs have been manufactured in tungsten (due to its high-attenuation coefficient[3,4]), the grid utilized for this study was printed with lower-density cobalt-chrome alloy. Cobalt-chrome was selected because of its wider availability in the metal 3D-printing industry and sufficient x-ray attenuation coefficient for low diagnostic energies (i.e., 4.52 cm^{-1} at ~ 80 keV).[12,13] For clinical applications requiring higher energies (i.e. > 100 keV), the scatter-rejection capabilities of a cobalt-chrome grid might not be sufficient. Fortunately, additive manufacturing using tungsten is becoming more commonly available.[14] We anticipate that our adaptive-gain methodology will be as effective when implemented with a tungsten grid, and is likely to benefit from the additional scatter rejection characteristics of more highly attenuating 2D-ASGs.

4.4 Summary

2D-ASGs are a promising scatter-rejection technique that improves soft-tissue contrast and reduces CT number inaccuracies in CBCT systems. GLA associated with the implementation of 2D-ASGs can lead to ring-artifacts in CBCT reconstructions. We present a novel implementation of an exposure-dependent adaptive-gain correction and Fourier-notch filtering scheme to reduce ring artifacts caused by 2D-ASG in a clinically representative cone-beam CT system. Our results suggest that proper characterization of the exposure-dependent response of GLA-affected pixels plays an important role in GLA correction. We also demonstrate that when rings are adequately corrected, CBCT reconstructions present enhanced CNR and CT-number accuracy. We believe our image-processing strategy eliminates some of the difficulties of 2D-ASG implementation in CBCT systems, and has the potential to make hardware-based scatter rejection techniques more feasible.

ACKNOWLEDGEMENTS

Support for this project came from the Canadian Institutes of Health Research and the Ontario Research Fund (Research Excellence). D.W.H. is the Dr. Sandy Kirkley Chair in Musculoskeletal Research within the Schulich School of Medicine & Dentistry at Western University.

REFERENCES

[1] Rührnschopf and EP, Klingenbeck K., “A general framework and review of scatter correction methods in cone beam CT. Part 2: scatter estimation approaches,” Medical physics. 38(9), 5186-5199 (2011).
[2] Rührnschopf EP, Klingenbeck K., "A general framework and review of scatter correction methods in x-ray cone-beam CT. Part 1: Scatter compensation approaches," Medical physics. 38(7), 4296-4311 (2011).
[3] Alexeev T, Kavanagh B, Miften M, Altunbas C., "Two-dimensional anti-scatter grid: A novel scatter rejection device for Cone-beam computed tomography," Medical physics. 45(2), 529-534 (2018).
[4] Altunbas C, Kavanagh B, Alexeev T, Miften M., "Transmission characteristics of a two-dimensional anti-scatter grid prototype for CBCT," Medical physics. 44(8), 11 (2017).
[5] Holdsworth DW, Cobos SF, Nikolov HN, Pollmann SI., "3D-printed anti-scatter collimators for artifact reduction in cone-beam CT," Paper presented at: SIAM Conference on Image Science, Bologna - Italy (2018).
[6] Alexeev T, Kavanagh B, Miften M, Altunbas C., Alexeev, Timur, et al. "A novel total variation based ring artifact suppression method for CBCT imaging with two-dimensional anti-scatter grids," Medical physics. 46(5), 2181-2193 (2019).
[7] Altunbas C, Lai CJ, Zhong Y, Shaw CC., "Reduction of ring artifacts in CBCT: Detection and correction of pixel gain variations in flat panel detectors," Medical physics. 41(9) (2014).
[8] Chakraborty D, Tarafder MK, Banerjee A, Chaudhuri SB., "Gabor-based spectral domain automated notch reject filter for quasi-periodic noise reduction from digital images," Multimedia Tools and Applications. 78(2), 1757-1783 (2019).
[9] Petrov IE, Nikolov HN, Holdsworth DW, Drangova M., "Image performance evaluation of a 3D surgical imaging platform," Paper presented at: Medical Imaging 2011: Physics of Medical Imaging (2011).
[10] Fokas G, Vaughn VM, Scarfe WC, Bornstein MM., "Accuracy of linear measurements on CBCT images related to presurgical implant treatment planning: A systematic review," Clinical oral implants research. 29, 393-415 (2018).
[11] Cho, Youngbin, et al., "Accurate technique for complete geometric calibration of cone-beam computed tomography systems," Medical physics. 32.4, 968-983 (2005).
[12] Ciurana, Joaquim, Luis Hernandez, and Jordi Delgado., "Energy density analysis on single tracks formed by selective laser melting with CoCrMo powder material," The International Journal of Advanced Manufacturing Technology. 68, 5-8, 1103-1110 (2013)
[13] Hubbell, John H., "Table of X-ray mass attenuation coefficients and mass energy absorption coefficients from 1 keV to 20 MeV for elements Z= 1 to 92 and 48 additional substances of dosimetric interest," US Department of Commerce, National Institute of Standards. NISTIR 5632 (1996).
[14] Guo, Meng, et al., "Formation of scanning tracks during Selective Laser Melting (SLM) of pure tungsten powder," International Journal of Refractory Metals and Hard Materials. 79, 37-46 (2019).